Sources with Significant Astrometric Offsets Between the S/X and K-band Celestial Frames

Aletha de Witt[1], Christopher S. Jacobs[2], David Gordon[3], Lucas Hunt[3], Megan Johnson[3]

Abstract The latest astrometric celestial reference frame (CRF) solutions at S/X-band and K-band have 1,014 sources in common, of which 36 are outliers with significant differences between the X- and K-band coordinates. We investigate possible astrophysical reasons for the large differences seen for the 36 outlier sources. These large differences may indicate significant structural differences between S/X and K-band. In order to study the astrophysical differences, we conducted multi-epoch, quasi-simultaneous S/X and K-band astrometric and imaging observations using the Very Long Baseline Array (VLBA). These images allow us to directly compare the source structure at X- and K-band, and to compare the direction of the extended emission from our imaging to the astrometric offset direction obtained from our CRF solutions.

Keywords Astrometry, VLBI, ICRF, AGN, jets, X-band, 8 GHz, K-band, 24 GHz

1 Introduction

Comparing the latest S/X (2022 Mar 05) and K-band (2022 Feb 07) astrometric celestial reference frame (CRF) solutions (using data back to 1980 for S/X and 2002 for K-band) produced by the United States Naval Observatory (USNO) shows 1,014 sources in common [1], of which 36 are outliers with at least one coordinate where the difference between S/X and K-band is $> 5\sigma$. Of the 36 outliers, there are three sources where the difference in δ are > 5 mas. We believe that these large differences may indicate significant structural differences between X- and K-band.

VLBI images show that Active Galactic Nuclei (AGN) tend to be more core-dominated at higher radio frequencies (e.g., [2]), as the extended structure in the jet tends to fade away with increasing frequency. The main reason why the apparent source structure is a function of frequency in AGN is rooted in their frequency dependent opacity, in particular from synchrotron self-absorption. Typically the core (or base) of an AGN jet is optically thick and has a flat or inverted radio spectra, while the jet is optically thin and has a normal or steep radio spectra. Frequency dependent opacity effects in AGN can also contribute to the frequency dependent shift of the VLBI core position ("core-shift"), with the core or base of the jet moving closer to the central black hole as the frequency increases, e.g., [3]. On the other hand, going to lower frequencies reduces the resolution available to detect structure, thereby desensitizing the baseline to structure. Thus, for some sources, we may only start to resolve individual components at higher radio frequencies.

We investigated possible astrophysical reasons for the large differences seen between the X- and K-band coordinates. We believe that these large differences may indicate significant structural differences between X- and K-band. For this reason we conducted special multi-epoch, quasi-simultaneous S/X and K-band astrometric and imaging observations between September 2020 and June 2021, using the Very Long Baseline Array (VLBA). From these observations we produced high-resolution images from which we derive source structure measures such as the radial extent and structure index, allowing us to directly compare the struc-

1. South African Radio Astronomy Observatory
2. Jet Propulsion Laboratory, California Institute of Technology
3. U.S. Naval Observatory

Table 1 Details of the S/X and K-band VLBA Observations.

Band	Date (2021)	Ref. Freq. (GHz)	Data Rate (Gbps)	Bandwidth	Polarization	$\theta_{\rm VLBA}$ (mas)
S/X-band	16 Apr, 24 May, 13 Jun	2.316	2	4×32 MHz	RCP	3.12
	–	8.668	–	12×32 MHz	–	0.82
K-band	18 Apr, 23 May, 12 Jun	23.568	4	4×128 MHz	RCP/LCP	0.30

ture at X- and K-band. In addition, we compare the direction of the extended emission obtained from model fitting to the astrometric offset direction obtained from the $\alpha\cos\delta$ and δ components. In this paper we present preliminary results from our investigation for 16 of the 36 outlier sources from the sessions that have been imaged so far.

2 Observations, Imaging and Model Fitting

In order to investigate the frequency dependent differences in source structure we conducted a series of ten quasi-simultaneous, multi-epoch S/X and K-band astrometric and imaging observations between September 2020 and June 2021 using the VLBA [4]. The observations were each 24 hours in duration and the data were correlated with the DiFX [5] software correlator at the Array Operations Center in Socorro, New Mexico. The S/X sessions were recorded in right circular polarization with a total data rate of 2 Gbps, and the K-band sessions in dual polarization with a total data rate of 4 Gbps. Data reduction and imaging have been completed thus far for the three S/X and K-band sessions observed between April and June 2021. The details of the observing dates, reference frequencies, observing modes, and angular resolution are given in Table 1.

The data were calibrated in the standard manner with the NRAO's Astronomical Imaging Processing System (AIPS) [6], using a semi-automated approach. An automated pipeline was used for self-calibration, deconvolution (using the standard CLEAN algorithm [7]), and imaging using the Caltech Difference Mapping software (DIFMAP) [8]. Images were produced for a total of 453 sources at X-band and 448 sources at K-band, with some sources having images at multiple epochs.

In addition to the imaging, we also fit a simple two-component, circular Gaussian model to the calibrated visibilities for each source using the MODELFIT task in DIFMAP to get an estimate of the offset and direction of the second brightest component. Estimates of the principal angle of extension of the total emission region ("jet direction") were obtained by fitting a line, going through (0,0), to the CLEAN component locations using a PYTHON script. This method was used to perform both an unweighted and flux-density-weighted fit. Details of our model fitting methods are described in [9].

3 Analysis

3.1 Astrometric Results

Comparing the latest CRF astrometric solutions produced by the USNO at S/X (sx-usno-220305) and K (k-usno-220305) shows 1,014 sources in common with at least two observations and $\sigma < 50$ nrad (~ 10 mas). Comparing the differences in the X- and K-band coordinates from these two catalogs shows 36 outliers with at least one coordinate where the difference is $> 5\sigma$. Note that there is a residual $\Delta\delta$ versus δ slope $= -1.3 \pm 0.1$ μas/deg that was not removed before taking the differences. Removing the 36 outliers leaves 978 sources in common with median inflated position errors of 46 μas in $\alpha\cos\delta$ and 60 μas in δ for X-band and 48 μas in $\alpha\cos\delta$ and 84 μas in δ for K-band.

From the 36 outliers there are three sources where the difference in the X−K coordinates in δ are > 5 mas. The radial X−K offsets of the 36 outliers range between 0.3 and 35 mas. Images have been produced for 16 of the 36 outliers from the observations listed in Table 1, and the radial X−K offsets for this subset of 16 outlier sources range between 0.3 and 2.73 mas.

3.2 Structure Metrics

We evaluate and compare the structure for each source at X- and K-band using various image-based source

structure metrics calculated from the image CLEAN component models (cf. [9]). The flux-density weighted radial extent (R) provides a measure of the source compactness by considering the extent of the source structure weighted by flux density. The median value of R over all sources is 1.82 mas for X and 0.86 mas for K-band, and over the 16 outliers the median values are 5.94 mas for X-band and 3.20 mas for K-band. The structure index (SI) is derived from the median value of the structural delay for each CLEAN component and each intermediate frequency (IF) channel for all possible projected VLBI baselines that could be observed on Earth [10, 11]. The SI indicates the magnitude of the structure of the source: the smaller the SI value, the lower the effect of the source structure, with values of SI > 3 indicating significant source structure. The median value of SI over all sources is 2.36 for X and 1.96 for K-band, and over the 16 outliers the median values are 4.01 for X-band and 3.18 for K-band. These results show that, on average, K-band relative to X is more compact, with the outliers having more extended structure.

3.3 Astrometric Offsets versus Jet Directions

We compare the X-K astrometric offset angle to the angle of the extended emission in the X- and K-band images for all 16 of the outlier sources. We assume that the K-band astrometric position is located at the peak of the K-band image and that the K-band core (versus X-band) would be closer to the central black hole. Thus, we measure the astrometric offset position and angle from the K-band phase center. Table 2 lists for each of the 16 outliers the X-K astrometric offset angle (AOA), the angle of the second brightest X- and K-band component obtained from the model fitting in DIFMAP (DMF), and the principal angle of extension of the X- and K-band total emission region from the flux-density-weighted fit to the CLEAN component locations (wCCF).

We find four sources where all three angles (i.e., the astrometric angle and the angle of the extended emission in the X- and K-band images) agree reasonably well, and five sources where the astrometric offset angle agrees with the angle of the extended emission from the K-band image, but the angle of the extended emission in the X-image is different. There are three sources where the angle of the extended emission in the X- and K-band images agree, but the astrometric offset angle is different. Where the angles don't agree, we find that in most instances the directions are anti-parallel to each other. There are also three sources where none of the angles agree, but in this case the images are all of poor quality and thus our jet direction is poorly determined.

Table 2 X-band versus K-band Offsets (all angles in degrees).

Source	X-K AOA	X DMF	X wCCF	K DMF	K wCCF
0112−017	114.9	130.3	130.0	132.2	132.6
CTA21	−9.9	–	–	–	–
3C84	−169.2	−173.0	−176.6	162.2	173.5
0723−008	−55.6	−8.8	−23.9	152.1	152.3
0729−222	−82.8	−94.2	−93.7	80.8	−109.1
0850+581	133.0	143.9	149.4	152.6	151.6
1156−094	124.3	−87.8	−88.0	–	−90.1
1214+588	115.5	118.9	118.4	−59.1	−58.4
3C286	−142.8	48.0	–	51.3	50.1
OQ208	50.0	23.9	30.1	–	118.3
3C309.1	−29.3	169.3	169.2	168.3	166.2
1600+335	−168.1	15.3	16.7	−3.8	−1.1
1710-269	131.9	78.0	−101.2	−87.2	−90.2
2037−253	−102.6	−69.4	−62.1	129.3	−19.4
2128−123	−150.4	−151.9	−149.3	−151.0	−150.9
3C454.3	−118.0	−106.4	−107.9	−72.5	−79.2

Figures 1 and 2 show two examples of sources for which all three of the angles agree reasonably well. The source 0112−017 (Figure 1) shows the astrometric offset position almost coinciding with the position of the second brightest component identified from the DIFMAP model fitting. Assuming that the astrometric position at X-band is located at the peak of the X-band image, this would imply that the X-band peak coincides with the weaker K-band jet component, with the peak emission at X-band being further down the jet. The source 2128−123 (Figure 2) is another example where all three angles agree reasonably well. For this source, the astrometric offset position (shown in the K-band image) is actually hidden behind the model-fit component.

Figure 3 shows the source 1214+588 as an example where the astrometric offset angle agrees with the angle of extended emission in the K-band image, but the angle of extended emission in the X-band image is different. However, we see that the angle of extended emission in the X-band image is in a direction anti-parallel to the K-band direction, with the angles

within a few degrees of 180° separation. For the source 1214+588 (and others where the X-band angle is in an anti-parallel direction) the X-band core appears to be the weaker X-band emission, and we suspect that we are mis-identifying the X-band core by assuming that the strong component is the core.

The source 3C309.1 (Figure 4) and 1156−094 are examples where the angle of extended emission from X and K images agree, but the astrometric offset angle is different, although we find that it is in a direction anti-parallel to the extended emission. Both sources appear to have very little extended emission, also seen from other epoch images at K-band [9].

4 Conclusions

Comparison of our most recent CRF astrometric catalogs shows 36 of 1,014 sources have statistically significant detections of astrometric offset. Sixteen of the 36 outliers have images at both X- and K-band, from multi-epoch, quasi-simultaneous S/X and K-band astrometric and imaging observations using the VLBA. Structure metrics derived from the image CLEAN component models show that the outliers tend to be the sources with more extended structures. The comparison of both imaging and astrometric results shows that large astrometric offsets have a strong tendency to be aligned along the jet direction of the source. Where the angles do not line up because they are anti-parallel, we suspect that the core may not be the strongest component in one of the images.

Future work: The next step will be to complete the imaging of the remaining seven quasi-simultaneous S/X and K-band VLBA observing sessions enabling the comparison of source structure and astrometric offset positions for the remaining 20 outlier sources.

Acknowledgements

The S/X results made extensive use of the International VLBI Service (IVS) data sets [12]. The S/X and K-band data sets also made extensive use of the VLBA [4] which is managed by the National Radio Astronomy Observatory (NRAO), funded by the National Science Foundation (NSF), and operated under cooperative agreement by Associated Universities. The authors gratefully acknowledge use of the VLBA under the USNO's time allocation. This work supports USNO's ongoing research into the celestial reference frame and geodesy. AdW was supported by the South African Radio Astronomy Observatory (SARAO), a facility of the National Research Foundation (NRF) of South Africa. DG, LH, and MJ were supported by the U.S. Naval Observatory (USNO). CJ's work was supported by the Jet Propulsion Laboratory, California Institute of Technology, under a contract with the National Aeronautics and Space Administration (80NM0018D0004).

References

1. Gordon, D., de Witt, A. & Jacobs, C. S., 12th IVS General Meeting, Helsinki, Finland (virtual), 31 Mar 2022. Current CRF Status at X/S and K Bands.
2. Charlot, P., et al., AJ, 139, 5, 1713–1779, 2010. The Celestial Reference Frame at 24 and 43 GHz. II. Imaging.
3. Sokolovsky, K. V., et al., A&A, 532, A38, 2011. A VLBA survey of the core shift effect in AGN jets.
4. Napier, P. J., in ASP Conf. Series, Zensus, J. A., Diamond, P. J., Napier, P. J., Eds.; ASP: San Francisco, CA, USA, 82, p. 59, 1995. VLBA Design.
5. Deller, A. T., et al., PASP 119, 318, 2007. DiFX: A Software Correlator for VLBI Using Multiprocessor Computing Environments.
6. Greisen, E. W., ed. A. Heck, 285, Dordrecht: Kluwer Academic Publishers, 109–125, 2003. AIPS, the VLA, and the VLBA.
7. Hogböm, J. A., A&A suppl., 15, 417, 1974. Aperture Synthesis with a Non-Regular Distribution of Interferometer Baselines.
8. Shepherd, M. C., in ASP Conf. Series, vol. 125, eds. G. Hunt and H. Payne, 77, 1997. Difmap: an Interactive Program for Synthesis Imaging
9. de Witt, A., et al., 'The Celestial Reference Frame at K-band: Imaging. I. The First 28 Epochs.', AJ, 2022, in press.
10. Fey, A. & Charlot, P., ApJ Suppl., 111,1, 95–142,1997. VLBA Observations of Radio Reference Frame Sources. II. Astrometric Suitability Based on Observed Structure.
11. Shabala, S., et al., J. Geod., 89, 9, 873–886, 2015. Simulating the effects of quasar structure on parameters from geodetic VLBI.
12. Schuh, H. & Behrend, D., J. Geodyn., 61, 68–80, 2012. VLBI: A fascinating technique for geodesy and astrometry.

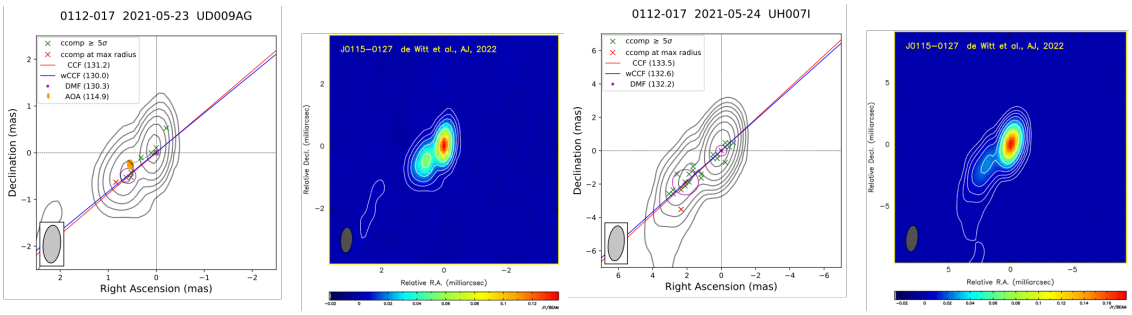

Fig. 1 Contour maps (in grey) and images of 0112−017 (J0115−0127) at K-band (left) and X-band (right).

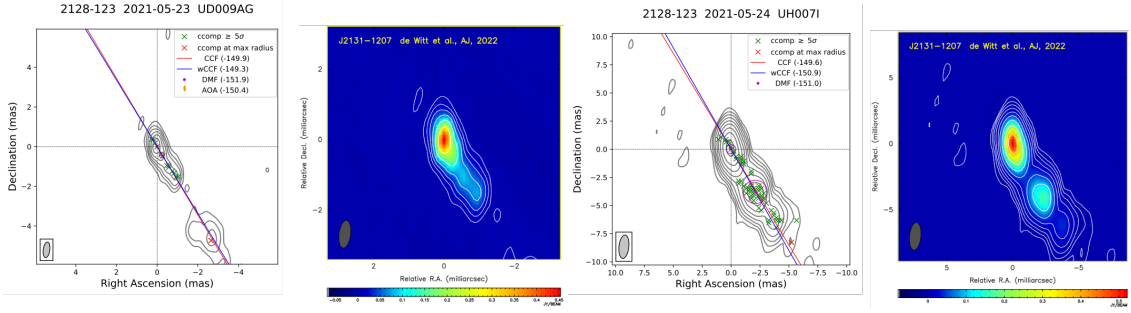

Fig. 2 Contour maps (in grey) and images of 2128−123 (J2131−1207) at K-band (left) and X-band (right).

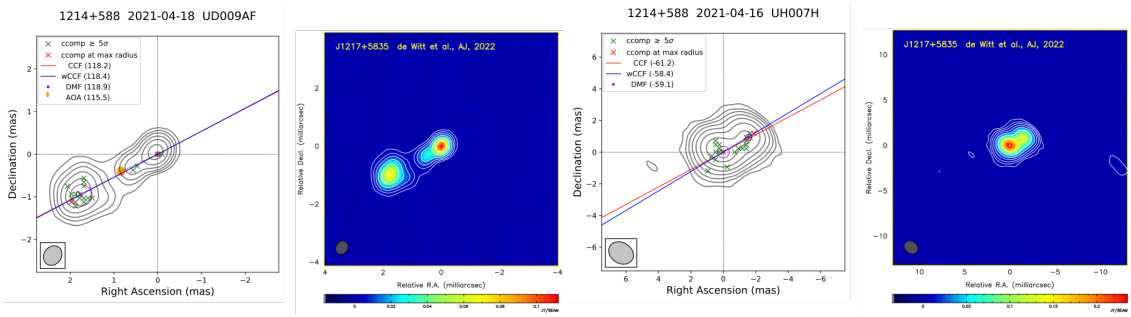

Fig. 3 Contour maps (in grey) and images of 1214+588 (J1217+5835) at K-band (left) and X-band (right).

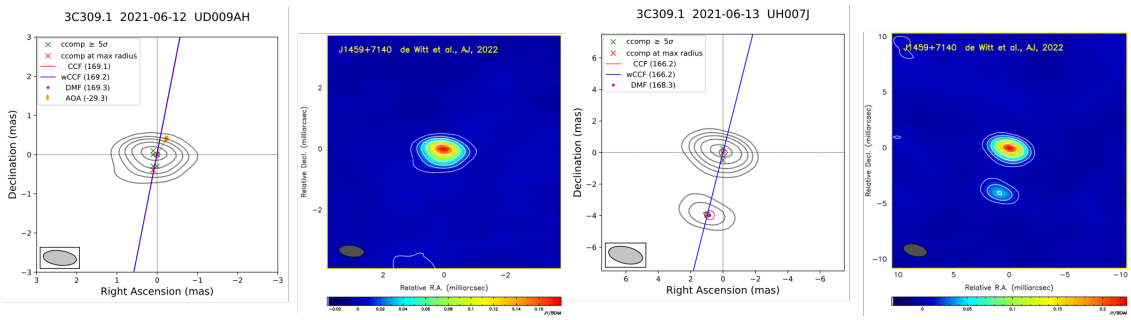

Fig. 4 Contour maps (in grey) and images of 3C309.1 (J1459+7140) at K-band (left) and X-band (right). Contour maps are overlaid with the line of best fit from the unweighted (CCF, blue line) and flux-density-weighted (wCCF, red line) linear fits through the locations of the image CLEAN components. The image CLEAN components (ccomp) are indicated with green crosses and the component with maximum distance from the phase center is indicated by a red cross. The position and size of the DIFMAP model-fit components (DMF) are indicated with magenta circles. The position of the astrometric offset angle (AOA) is indicated with a yellow ellipse with the minor and major axis representing the error in the $\alpha \cos \delta$ and δ differences. Position angles are given in the plot legend.